Prediction of moisture transfer in cement-based materials: Use of a porous network model to access transfer parameters

Mohamed Abdou Ibro, Jérôme Verdier, Sandrine Geoffroy, Hugo Cagnon, Xavier Bourbon

Version of Record: https://www.sciencedirect.com/science/article/pii/S0008884620315908
Manuscript_511fa74b29f8acc02ba8649ba0754e87

Prediction of moisture transfer in cement-based materials: use of a porous network model to access transfer parameters

Mohamed Abdou Ibro [a,1], Jérôme Verdier [a,2], Sandrine Geoffroy [a], Hugo Cagnon [a], Xavier Bourbon[b]

[a]Université de Toulouse, UPS, INSA, LMDC (Laboratoire Matériaux et Durabilité des Constructions),135 avenue de Rangueil, F-31077, Toulouse Cedex 4, France

[b]Andra Parc de la Croix Blanche, 1-7 Rue Jean Monnet, F-92298, Chatenay Malabry, Cedex, France

[1]abdouibr@insa-toulouse.fr

[2] verdier@insa-toulouse.fr

Abstract

Knowing the water transport phenomena is fundamental for understanding the durability of cement-based materials. The moisture content within cementitious materials is of primary importance because it has a direct influence on mechanical (shrinkage, creep) and chemical (penetration of aggressive agents) degradation. Many models based on the determination of the transfer properties of the material under study already exist but require fitting of the parameters to find the experimental kinetics. Transfer parameters are generally estimated from the empirical approaches developed for soils by Van Genuchten and the water vapour diffusion reduction factor is often calculated via Millington's semi-empirical model. In this paper, we make a proposal to improve the prediction of moisture transfer, through mechanisms such as drying, capillary imbibition and water vapour permeability in cement-based materials, by using a porous network model to access the transfer parameters.

1 Introduction

In order to ensure the durability of civil engineering structures, it is essential to understand and predict water movement in those porous materials, particularly in relation to the environment. We can mention, for example, structures for the storage of radioactive waste, which are subjected to drying phenomena during the exploitation phase and then resaturation by the surrounding environment. These water movements are thus responsible for the transport of aggressive agents through the cementitious materials, which can take place in gaseous form (carbon dioxide) or via aqueous liquid (chloride ions, sulfates). Ishida [1] explains that the moisture transport in the pores of cementitious materials can be described in different ways. The most fundamental features are the transport of liquid water described by Darcy's law and the transport of water vapour described by Fick's law. In the literature, the modelling of moisture transport in cement-based materials generally focuses on the drying process, which is the main cause of moisture content change. Modelling of the drying of porous materials is

often approached by assuming that the gas pressure of the vapour-air mixture remains constantly equal to the atmospheric pressure [2]–[5]. These approaches consider a simple non-linear diffusion equation using a water diffusion coefficient called water diffusivity. Mainguy et al. [6], [7] show the difficulty of evaluating the importance of each transfer phenomenon from water diffusivity alone and thus develop a multiphase model considering gas pressure variations based on the movements of the gas phase and liquid water. However, even for this more complete approach, it is necessary to adjust an important transfer parameter, the intrinsic liquid permeability, by inverse analysis of the experimental drying kinetics. In addition, these kinetics are more generally found with aberrant values of intrinsic liquid permeability. This is in line with the findings of Thiery et al. [8], who have shown that the gas phase transfer laws chosen by Mainguy et al. [6] are not suitable for concrete and therefore propose a new set of laws for the gas permeability and water vapour diffusion coefficient, based on experimental results obtained for different degrees of saturation. It is therefore essential to correctly evaluate the transfer parameters specific to the materials studied in order to predict moisture transfers correctly in cement-based materials. Many contributions are available regarding the modelling of liquid and gas transfer, highlighting significant variations and necessary adjustments of the transfer parameters.

Many researchers have developed water transfer models for cementitious materials. Bazant and Najjar [2] showed the dependence of diffusivity on pore moisture, degree of hydration and temperature in concrete analytically. In this model, the moisture diffusivity and moisture capacity are treated as separate parameters evaluated from independent test results. Xi et al. [3] developed a semi empirical expression for the sorption isotherm that improved on Bazant and Najjar's model [2]. Bonnet [34], Francy [35], West and Holmes [4], Leivo and Rantala [5] have proposed modelling how the porous materials dry by assuming that the gas pressure of the vapour-air mixture remains constantly equal to the atmospheric pressure. These approaches consider a simple non-linear diffusion equation using a water diffusion coefficient called water diffusivity ($D(S_w)$):

$$\frac{\partial S_w}{\partial t} - \mathrm{div}[D(S_w).\mathrm{grad}\,(S_w)] = 0 \qquad (1)$$

The water diffusivity, which is a function of the degree of water saturation (S_w), reflects the different modes of moisture transport. Some authors have evaluated this coefficient on the basis of experimental data [3], [36]–[39]. The limitation of all these models is that they are based on observations made on soils (more rarely porous rocks such as some sandstones) or on consolidated materials but rarely on porous materials such as concrete. Mainguy et al. [6], [7] explain that the assumption of a constant gas pressure is common in soil mechanics and relies upon a familiar idea. Because of the assumed high conductivity of the vapour-air phase, any change in its pressure, whatever the origin, returns quasi-immediately to equilibrium because of Darcean air transport that occurs with kinetics far higher than the other transfer phenomena. With this assumption, the drying process can be modelled with a

standard diffusion equation involving either the liquid-water content or the vapour pressure. By modelling the drying of different cement based-materials Mainguy et al. [6], [7] showed that the modelling at constant total gas pressure reflected a drying process that had taken place too quickly compared to the experimental drying kinetics. In conclusion, these authors did not succeed in explaining the discrepancies between the experimental data and the modelled processes. Among their conclusions, they highlighted the difficulties in quantifying the weight of each water transfer phenomenon properly. They thus developed a multiphase model considering the total gas pressure evolution and taking the coupled movements of water (liquid and vapour) into account. For all these reasons, we have chosen to use a multiphase model considering gas pressure variations in our study for all the simulations carried out.

On the basis of Mualem's research [9], Van Genuchten [10] has proposed analytical relations derived from desorption isotherms to predict both liquid and gas permeabilities for soils and many other authors have developed models to predict liquid and gas permeabilities from porous network models [11]–[16]. To describe the vapour diffusion contribution in the moisture transport of unsaturated materials, a water vapour diffusion reduction factor, noted as R_d, is commonly considered as a function of saturation [17], [18] to correct the flow of vapour through the porous material. For granular materials, Millington [19] has proposed an equation that takes the microstructure of the material into account, in addition to saturation. Saetta et al. [20] have proposed the *S-shaped curve* relation of diffusivity at a given relative humidity (RH). The water vapour sorption/desorption isotherm is a key parameter associated with the moisture transport properties. Philippi and Souza [21] have developed a 3D-scale geometric model of moisture retention and isothermal transfer in a cement and lime mortar. It is based, essentially, on a texture analysis performed on images of polished sections of the sample material, taken using a scanning electron microscope. Ishida et al. [22] generalize a moisture transport model and a moisture equilibrium model with respect to temperature and drying-wetting history by taking the hysteresis phenomena in nanometer to micrometer scale pores into account. Most recently, Jiang et al. [23] have developed a model for predicting water vapour sorption hysteresis of cement-based materials based on pore size distributions and pore networks, considering the difference of liquid-gas interfaces between the sorption and desorption processes. Also, in this model, the water contents in C-S-H interlayers and gel/capillary pores are considered separately. De Burgh et al. [24] have proposed a physical model for water vapour sorption isotherms based on established thermodynamic principles, applied to a predicted microstructure. This model is built on a modern form of the cement-hydration model of Powers and Brownyard [25]. Ranaivomanana et al. [26], [27] have developed a porous network model to predict hysteresis phenomena in water vapour sorption isotherms and proposed new methods for calculating transport factors based on physical and statistical considerations.

There are many experimental studies of moisture transfer through porous materials that evaluate the evolution of moisture content using a gravimetric method [28]–[30]. This method allows accurate measurements of the total amount of water, but its distribution cannot be established. Thus, many authors have developed non-destructive techniques (NDT), such as electrical resistivity [31]–[33], to observe how the degree of water saturation varies spatially through the specimen. This parameter is strongly conditioned by the water saturation and composition of the interstitial aqueous phase, with very accessible evaluation techniques, hence the particular interest given to this technique, which will be used in this study.

The aim of this article is to propose an appropriate approach for the modelling of several mechanisms of moisture transfers in cementitious materials, based on a porous network model for the prediction of transfer parameters developed by Ranaivomanana et al. [26], [27]. Some of the experimental data used in the present paper were collected from the literature to complete a full data set for drying kinetics modelling and thus verify the validity of the kinetics and the parameters predicted by the different approaches. An experimental campaign involving the main phases of moisture transfer was also carried out in this study. Thus, drying, capillary imbibition and water vapour permeability experiments were performed in order to validate the predictions of the porous network model concerning the transfer parameters. The numerical simulations of moisture transfer experiments were run for three different series of cement based-materials. This study shows different evolution of kinetics according to the approach considered for the input parameters. The results of the simulations are compared to the experimental results, showing good agreement between the model and the experimental data, with few adjusted parameters. This numerical campaign coupled with the experimental results also allows discussion of the different kinetics obtained from the differences observed in the evolution of the input parameters estimated by various approaches.

2 Multiphase model used in this study

2.1 Assumptions and constitutive equations

Based on a thermodynamic approach to mass transfer in continuous porous media developed by Coussy et al. [40], [41], Mainguy et al. [6] have developed a multiphase model where moisture transfers are described by the movements of the gas phase and liquid water. In this model, the solid skeleton is considered to be non-deformable, the liquid phase incompressible, the forces of gravity negligible and the water transfers isothermal at 20 °C. The gas phase consists of a mixture of two perfect gases, dry air of partial pressure P_a and water vapour of partial pressure P_v. The total pressure, P_g, of the mixture is assumed to be ideal:

$$P_g = P_a + P_v \quad (2)$$

The macroscopic mass conservation equations of each mobile component present in the porous media are:

$$\begin{cases} \dfrac{\partial(\emptyset S_l \rho_l)}{\partial t} = -div\overrightarrow{w_l} - \dot{\mu} \\ \dfrac{\partial[\emptyset \rho_v (1 - S_l)]}{\partial t} = -div\overrightarrow{w_v} + \dot{\mu} \\ \dfrac{\partial[\emptyset \rho_a (1 - S_l)]}{\partial t} = -div\overrightarrow{w_a} \end{cases} \quad (3)$$

where ρ_i refers to the density of component i= *l, v* or *a,* the corresponding mass flow being w_i. $\emptyset$ and S_l refer to accessible porosity and liquid water saturation rate respectively. The quantities $[\emptyset\rho_v(1 - S_l)]$; $(\emptyset S_l \rho_l)$; $[\emptyset\rho_a(1 - S_l)]$ in the time derivation terms correspond respectively to the mass of water vapour, liquid water and dry air contained in a unit volume of material. Divergence operators for mass flows correspond to mass exchanges with the outside. Finally, $\dot{\mu}$ refers to phase changes, the mass of water that passes from the liquid phase to the gas phase and vice versa. The mass flow w_i is equal to the product of its mass m_i and its velocity *vi*.

The mass flow of the liquid water expressed by the generalized Darcy's law for unsaturated conditions is given by the following relationship:

$$\vec{w}_l = -\rho_l \frac{K_l}{\mu_l} k_{rl} \overrightarrow{grad} P_l \quad (4)$$

The mass flow of each gaseous component *i* ($\vec{w}_i$) is the sum of the convective flow ($\vec{w}_i^c$), governed by Darcy's law, and the diffuse flow ($\vec{w}_i^d$), governed by Fick's law:

$$\vec{w}_i = \vec{w}_i^c + \vec{w}_i^d \quad (5)$$

$$\vec{w}_i^c = -\frac{P_i M_i K_g}{RT\mu_g}\left(k_{rg} + \frac{\beta}{P_g}\right)\overrightarrow{grad} P_g \quad (6)$$

$$\vec{w}_i^d = -\frac{P_i M_i}{RT} D \overrightarrow{grad}\left(\frac{P_i}{P_g}\right) \quad (7)$$

K_i is the intrinsic permeability of fluid *i* (m^2); k_{ri} is the relative permeability of fluid *i* (-); R is the perfect gas constant (8.3144 $J.mol^{-1}.K^{-1}$); T is the temperature; M_i is the molecular weight of fluid i; and D is the diffusion coefficient of the gaseous components (m^2/s) .

2.2 *Identification of parameters required for modelling*

The key parameters for modelling moisture transfer are the accessible porosity, ∅, obtained experimentally; the liquid water saturation rate, S_l; the relative permeabilities to liquid, k_{rl}, and to gas, k_{rg} , and the diffusion coefficient of the gaseous components, *D,* of the tested materials. In order to continuously express the saturation rate S_l as a function of relative humidity, Mainguy et al. [6] use a function defined by Van Genuchten [10] in which *a* and *m* are calibration parameters.

$$P_c(S_l) = a\left(S_l^{1/m} - 1\right)^{1-m} \quad (8)$$

The relative permeabilities to liquid, k_{rl}, and to gas, k_{rg} , are approximated by the relationships obtained for soils by Van Genuchten [10] from Mualem's model [9].

$$k_{rl}(S_l) = S_l^{0,5}\left[1 - \left(1 - S_l^{\frac{1}{m}}\right)^m\right]^2 \quad (9)$$

$$k_{rg}(S_l) = (1 - S_l)^{0,5}\left(1 - S_l^{\frac{1}{m}}\right)^{2m} \quad (10)$$

Based on experiments carried out on cement-based materials, Thiery et al. [8] have shown, more recently, that the transfer laws chosen by Mainguy et al. [6] are not suitable for this type of materials. They therefore adopt modified expressions of k_{rl} and k_{rg} proposed by Monlouis Bonnaire [15].

$$k_{rl}(S_l) = S_l^{5,5}\left[1 - \left(1 - S_l^{\frac{1}{m}}\right)^m\right]^2 \quad (11)$$

$$k_{rg}(S_l) = (1 - S_l)^{5,5}\left(1 - S_l^{\frac{1}{m}}\right)^{2m} \quad (12)$$

The diffusion coefficient of the gaseous components *D* in the diffuse contribution of water vapour is given by the following relationship:

$$D = R_d D_o \quad (13)$$

where D_o is the free water vapour diffusion coefficient in the air. It is given by De Vries and Kruger's expression [42]. The vapour diffusion resistance factor corrects the flow of vapour through the material based on changes in the degree of saturation. This parameter is approached by Millington [19].

$$R_d(\emptyset, S_l) = \emptyset^a (1 - S_l)^b \quad (14)$$

As suggested by Millington, the values of a and b are respectively equal to 1.33 and 3.33 [19]. However, observing that these values lead to an overestimation of the diffusion coefficient, D, Thiery et al. [8], considering the fitting of experimental data, suggested the values of 2.74 for a and 4.2 for b. As mentioned above, many porous network models also provide access to these parameters necessary for transfer modelling. Millington [19], Saetta et al. [20], Philippi and Souza [21], and Ishida et al. [22], have developed porous network models to access liquid and gas permeability. Pradhan et al. [43] and Bejaoui and Bary [44] have developed porous network models to access diffusivity. In this study, we will use the porous network model developed by Ranaivomanana et al. [26], [27] to estimate the transfer parameters as this model, developed more recently, takes the key points from the previous work into account. Also, the model has already given coherent results on cement-based material.

3 Porous network model for predicting transfer parameters

3.1 Assumptions and constitutive equations

Ranaivomanana et al. [26], [27] have developed a physical model of a porous network for cementitious materials to predict water sorption and desorption isotherms. For situations involving drying-humidification cycles, this model can also predict the hysteresis between sorption and desorption. The model is based on an idealized pore size distribution with three modes, associated with C–S–H pores and with narrow and wide capillary pores. The wide capillary pores (third mode) are assumed to be made up of initially water-filled spaces ranging (air pores) from about fifty to hundreds nanometers but may also include microcracks having size larger than 1000 nm. The volume of this mode, associated with wide capillaries, is directly deduced from the sharp drop of the desorption isotherm at high RH. The first mode, corresponding to C–S–H pores, is calibrated by calculating the volume of C–S–H formed using the method proposed by Adenot [45]. It requires as input the formulation of the material and the degree of hydration (to quantify the amount of hydrated cement) and the chemical composition of the cement (to quantify the amount of hydrates formed from the amount of oxides). The volume of the second mode, corresponding to narrow capillary pores, is the complement needed to reach the water porosity, measured following the AFPC-AFREM procedure [46] (saturation under vacuum method). The model considers the BET theory of multi-molecular layered adsorption [47] to manage the adsorption of water molecules on the pore surface. Then, capillary condensation is managed by the Kelvin Laplace equation.

To model the isotherms while paying attention to the hysteresis effect, it was assumed that the drying of a pore was possible only if it was connected to the dry fraction of the pore network. As the hysteresis between desorption and sorption isotherms is explained by the presence of "ink-bottle" shaped pores, the drying of much of the pore volume is possible only at low RH. Assuming that drying

affects pores with size r_i when the relative humidity is h_i, the drained portion of the porous network represents a fraction of the pores of radius larger than r_i, the author describes connectivity as the probability of the interconnection of pores with a radius greater than r_i. Beyond isotherms, the model makes it possible to account for certain characteristics of the porous structure, including the specific surface area, and to predict permeability values for liquid and gas.

In most porous network models, the pore cross-section is considered as cylindrical. However, for the same volume, the smaller the cross section $a_p(r)$ of the pore is, the longer is its developed length. This has an impact on pore geometry. If the pores were considered to be cylindrical, the thinnest ones would have very long developed lengths. Then, they would provide the main connection between the larger pores and the dry network, which would lead to high hysteresis up to low relative humidity. Thus, as the C-S-H is present in the form of nanometric particles aggregated with one another, Ranaivomanana et al. [26], [27] attribute a flattened shape to pores with smaller radii, which is approximated by an oblong geometry (Fig. 1) of cross-section defined by:

$$a_p(r) = \left(4\left(A_p(r) - 1\right) + \pi\right)r^2 \quad (15)$$

$$A_p(r) = \frac{l}{2r} = min\left(exp\left(\frac{r_{cr}}{r}; 15\right)\right) \quad (16)$$

where $A_p(r)$ is the flattening coefficient defined as the ratio between the width of the pore cross-section and its height. r_{cr} is the critical radius (nm), which is a calibration parameter interpreted as a value of the radius that defines the passage from capillary pores to C-S-H pores. By inverse analysis carried out on different types of cementitious materials [26], the adequate value of the critical radius is found to be 2 nm. The large pores are therefore cylindrical since their flattening, A_p, cannot exceed 1 when r is large. The pores gradually become flattened as r decreases.

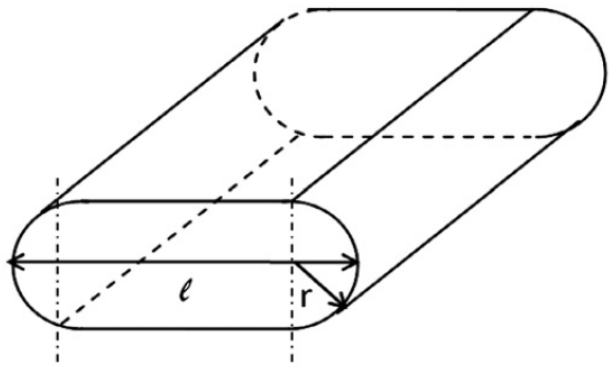

Fig. 1 Oblong shaped pore [26], [27]

3.2 Water transfer parameters

The relative permeabilities to liquid and gas are estimated from liquid and gas flows q_l and q_g based on a simple representation of the porous space with straight, parallel channels. For a porous network consisting of 3 families of pores assumed to be composed of N pores of different sizes, the relative permeabilities to liquid and gas, and the water vapour diffusion reduction factor R_d are determined by the following relationships [26], [27]:

$$K_{rl} = \frac{S_l \sum_{p=1}^{N} l(r)\, q_l(r) S_r^* F_l(RH)}{\sum_{p=1}^{N} l(r)\, q_l(r)} \quad (17)$$

$$K_{rg} = \frac{(1 - S_l) \sum_{p=1}^{N} l(r)\, q_g(r) S_r^* F_g(RH)}{\sum_{p=1}^{N} l(r)\, q_g(r)} \quad (18)$$

$$R_d = (1 - S_l) \sum_{p=1}^{N} l(r)\, a_p(r) \frac{F_g(RH)}{1 + \frac{\lambda}{2r}} \quad (19)$$

S_l refers to the liquid water saturation rate. The total developed length of all pores with radius r is denoted $l(r)$. Based on Poiseuille's law, $q_l(r)$ refers to the liquid flow rate through a pore of radius r_p under the effect of a pressure gradient. $q_g(r)$ is the total gas flow rate that considers the laminar flow (Poiseuille) and the molecular flow (Knudsen). S_r^* is equal to 1 if the pore family is fully saturated and 0 if the pore family is partially saturated or completely dry. For a given relative humidity, $F_g(RH)$ is the connectivity to drained percolation pathways of a dried pore size and $F_l(RH)$ is the connectivity of a saturated pore to saturated percolation pathways. λ is the mean free path of water vapour molecules in the air.

This model has been improved to better predict sorption phenomena from partially saturated states. For sorption at a given relative humidity, Ranaivomanana et al. [26], [27] consider the possibility of completely and directly saturating the family pores smaller than the Kelvin radius corresponding to this relative humidity. This family of pores is not completely saturated due in particular to the existence of ink-bottle-shaped pores. It would thus be necessary to reach a relative humidity higher than that corresponding to the kelvin radius to saturate the large part of these pores. In order to take this into account, we consider as a first approximation that a pore family will be completely saturated as soon as 90% of the pores of this family are saturated. An alternative to this first approximation would be to propose in a complementary study an evolutionary porous model (displacement and modification of the surfaces for the different modes). This allows us to better model the difficulty of resaturation of a pore due to its accessibility and the creation of damage during preliminary drying. Indeed, whatever the choice of preconditioning, the drying process generates microcracks [48]. This

microcracking and the drainage of the paste-aggregate interfaces will modify the pore network and the preferential pathways. Then the integration of this porous network model into Mainguy et al.'s [6] transfer model allows the hysteresis to be considered in the simulation of experiments involving sorption and desorption phenomena.

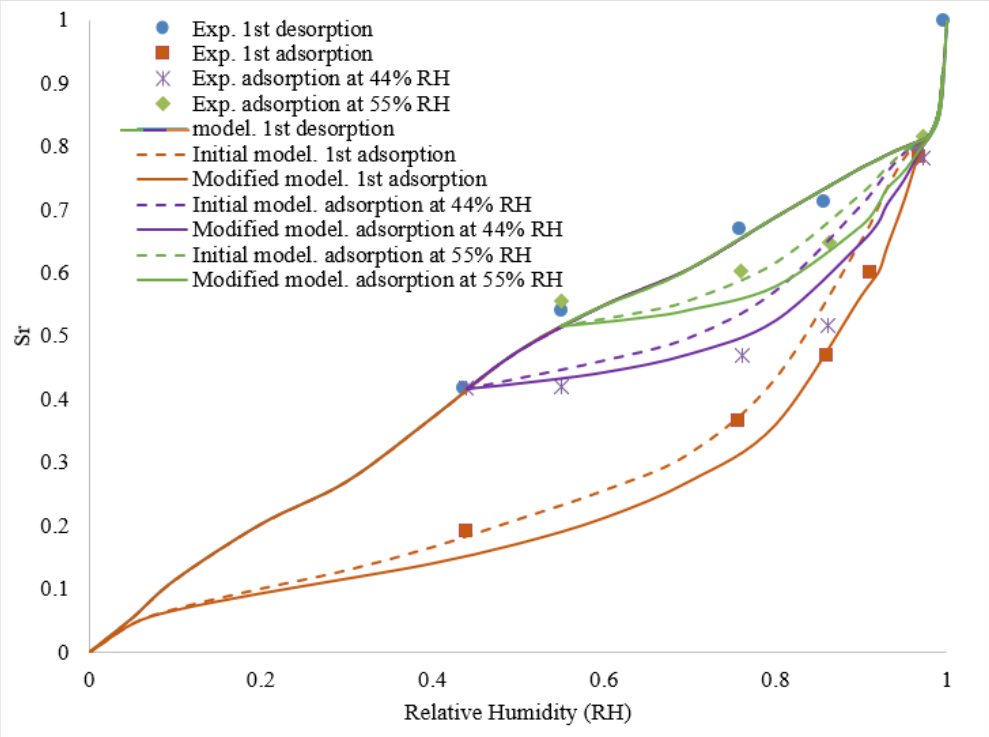

Fig. 2 Confrontation of sorptions for several cycles for a CEM I 52.5 concrete (B1)

4 Results and discussion

The experimental data found in the literature are presented in section 4.1. Our own experiments are presented in section 4.2 (drying combined with electrical resistivity monitoring, capillary imbibition and water vapour permeability experiments). This section concludes with simulations and discussions.

4.1 Experimental data from literature

Some of the experimental data used in this paper were collected from the literature [7], [49]–[52]. A total of eight formulations were tested, two cement pastes and six concretes, separated into two series. The first series of CEM I 52.5 cement-based materials, based on the work of Baroghel Bouny et al. [49], [51], [52] consisted of ordinary concrete (BO), very high performance concrete (BH) and the corresponding cement pastes, CO and CH. The second series included CEM I 52.5 (B1) and CEM V 42.5 (B2) concrete formulations as well as the "low hydration heat/low pH concretes" designed as candidate materials for use in a future deep geological radioactive waste disposal site [26]. The ternary binders of the two low pH concretes studied were composed of CEM I and two pozzolanic additives: silica fume, which was common to both, and fly ash (T1) or slag (T3) to complete the blend. Drying of this second series of materials was carried out in long-term experiments (almost two years), which is

rare in the literature, hence the interest of using this database. The mixture proportions and the main characteristics of the concretes and the cement pastes are summarized in Table 1.

Table 1: Mix-composition and main characteristics of test materials for series 1 and 2

Series reference	1				2			
Material reference	BO	BH	CO	CH	B1	B2	T1	T3
Gravel content (kg/m^3) (min/max grain size in mm)	1192 (4/20)	1265 (4/20)			945 (5/12.5)	984 (5/12.5)	185 (5/8) 850 (8/12)	185 (5/8) 850 (8/12)
Sand content (kg/m^3) (min/max grain size in mm)	744 (0/5)	652 (0/5)			858 (0/4)	800 (0/4)	813 (0/5)	813 (0/5)
Cement content (kg/m^3)	353	421			400	450	148	79
Silica fume content (kg/m^3)		42.1					128	128
Fly ash content (kg/m^3)							119	
Slag content (kg/m^3)								188
Superplasticizer (kg/m^3)		7.59			10	11.25	5.14	5.14
Water-to-cement ratio (W/C)	0.43	0.27	0.35	0.20	0.45	0.40		
Water-to-binder ratio (W/B)			0.35	0.18			0.40	0.43
Silica fume to cement ratio (SF/C)				0.10				
Water porosity (%)	12.2	8.2	30.3	20.4	12.3	14.4	15.2	16.6
Experimental gas permeability (10^{-17} m^2)	16 [53]	4 [53]			4	5.5	2.2 [54]	3.6 [54]
Experimental water permeability (10^{-19} m^2)					0.95	1.37	2.3 [54]	1.6 [54]

The drying experiments for the first and second series of materials are described in [49] and [50]. The temperature of the tests was set at 20°C and the lateral face of the sample was protected from water transfers by aluminium foil for series 1 and resin for series 2. It was then assumed that the drying was unidirectional. The test conditions are given in Table 2.

Table 2: Test conditions of tested materials for series 1 and 2

Series reference	1				2			
Material reference	BO	BH	CO	CH	B1	B2	T1	T3
Dimensions	Cylindrical test specimens Diameter:16 cm Height: 10 cm				Prismatic specimens Length: 6 cm Width: 3.5 cm Thickness: 5 cm			
Weight (kg)	4.9076	5.0436	4.1954	4.6647	0.2608	0.2391	0.2471	0.2432
Initial internal relative humidity RH_i (%)	90	65	85	75	100	100	100	100
External relative humidity RH_{ext} (%)	50				44			

4.2 Experiments

The experiments performed as part of this study were carried out on a third series of concrete materials. The formulations of these concretes, denoted B1* and B2*, were similar to the formulations of concretes B1 and B2, respectively, in Series 2. The difference lay in the nature and dosage of superplasticizer. Then the water to cement ratio was adjusted in the formulation of our materials in order to obtain the same properties as for B1 and B2 (series 3). The mixture proportions and the main characteristics of these concretes are summarized in Table 3. In addition to experimental data from the literature, drying combined with electrical resistivity monitoring, capillary imbibition and water

vapour permeability tests were also carried out in order to validate the relevance of the transfer parameters.

Table 3: Mix-composition and main characteristics of test materials for series 3

Series	3	
Material reference	B1*	B2*
Gravel content (kg/m3) (min/max grain size in mm)	945 (4/12)	984 (4/12)
Sand content (kg/m3) (min/max grain size in mm)	858 (0/4)	800 (0/4)
Cement content (kg/m3)	400	450
Superplasticizer (kg/m3)	3.2	4.5
Water-to-cement ratio (W/C)	0.43	0.38
Water porosity	0.132	0.128
Experimental intrinsic water permeability K_l (10^{-19} m^2)	0.93	1.45

4.2.1 Drying experiment coupled with electrical resistivity measurements

For the drying experiments, the temperature of the tests was set at 20 °C and the lateral face of the sample was protected from water transfers by resin, assuming that the drying was unidirectional. The cylindrical specimens, with a diameter of 11.2 cm and a height of 22.4 cm, initially saturated under vacuum, were placed in a climatic vessel at 8% relative humidity. The kinetics of mass losses over time was obtained by gravimetric evaluation. This method allowed accurate measurements of the total amount of mass loss at a certain time but its distribution could not be established. Local resistivity measurements were therefore carried out during drying to evaluate the evolution of saturation profiles within the material.

4.2.1.1 Resistivity measurement: principle and testing procedure

Electrical resistance R (ohm) was directly measured by the testing device using the direct application of Ohm's law (Fig. 3). When a current I (A) was applied between the two cross-sectional areas of a specimen using plate electrodes (injection electrodes), a potential drop ΔV (V) was measured between the two electrodes. Resistivity ρ (ohm.m) is an intrinsic characteristic of a material and is independent of the geometry of the specimen. Equation (1) describes the relationship between the resistivity and resistance:

$$\rho = k.R = k.\frac{\Delta V}{I} \quad With\ k = \frac{A}{L} \qquad (20)$$

where R is the resistance of concrete; and k (m) is a geometrical factor that depends on the size and shape of the specimen as well as the distance between the probes on the testing device; A is the cross-sectional area (m^2) and L is the length of the specimen.

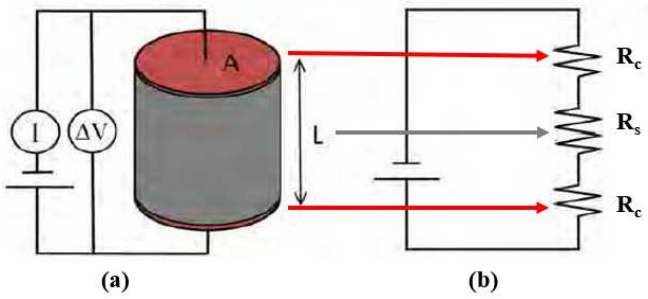

Fig. 3. Resistivity measurement diagram showing (a) the application of Ohm's law for specimens of uniform cross-section and (b) contact and specimen resistance [33].

To evaluate the overall resistivity of the specimens, two-point resistivity measurements were made on both sides of the cross-sections of the specimen. A device inspired by the multi-ring resistivity cell developed by Du plooy et al. [33] was set up to evaluate the local evolution of the resistivity in addition to the global resistivity. The new device consisted of 2 mm wide copper rings uniformly spaced over the height of the sample at intervals of 20 mm, thus allowing the potential drop between any two electrodes to be measured (Fig. 4). A copper-based conductive paint applied to the ring-concrete interface reduced contact resistance by ensuring continuous electrode-concrete contact, thereby ensuring test repeatability. In addition, this measuring device was interesting because it allowed a four-point Wenner measurement, which is the most common way to determine the resistivity of concrete [55]. Perforated plates used as injection electrodes were slightly embedded in the concrete to ensure better electrode-concrete contact. The injection electrodes were connected to a generator and the current used in the experimental campaign was alternating current at a frequency of 15 Hz. For all configurations tested, the current was always imposed on perforated plate electrodes as large as the cross-sectional area of the specimen. The geometric analytical factor defined by Ohm's law (Eq. (1)) was therefore valid for our entire study. Finally, saturation evolutions were obtained from the relationship between the degree of saturation and the electrical resistivity. Resistivity was measured at different degrees of saturation with a homogeneous distribution of humidity, as reported by many authors in the literature [33], [56].

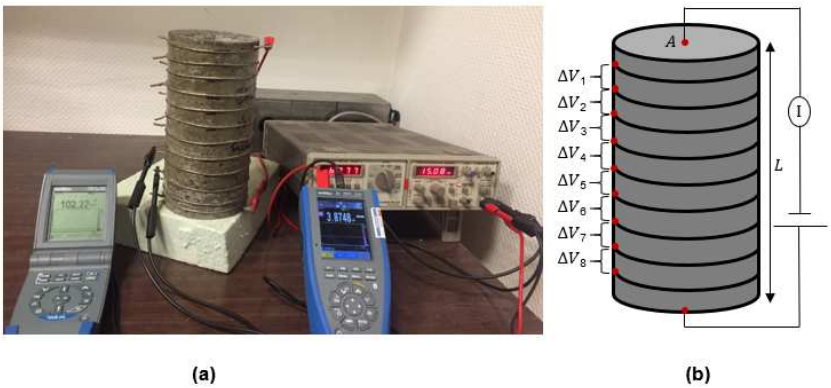

Fig. 4. Resistivity measuring device (a) and measuring principle (b) with copper rings

4.2.2 *Capillary imbibition experiment*

Imbibition tests were performed on 5 cm high cylindrical specimens 11.2 cm in diameter that had been subjected to a preconditioning procedure consisting of drying them completely and waterproofing their lateral faces with resin. The specimens are dried at 50°C to reach an overall saturation level of 30% and then at 80°C to reach the dry state (approximate overall saturation level of 6% considering that total free water is removed for drying at 105°C). We have chosen to take 80°C instead of 105°C as the reference temperature to avoid damaging the materials too much before testing [57]. Then, the bottom flat face of the specimens was brought into contact with water, only two millimetres below the water level, which was kept constant throughout the test period by an overflow system. The sample gained weight due to water rise, which was registered at regular time intervals to evaluate the rate of water absorption. Water absorption measurement is generally performed over a few hours, but it is necessary to study capillary imbibition over a longer period for materials used for long-term storage. So, in this study, the test was carried out until the mass stabilized (loss of mass between two weighing operations carried out at an interval of 24 hours ≤0.1%).

4.2.3 *Water vapour permeability experiment*

Vapour permeability refers to the ratio of the amount of vapour passing through a material per unit of thickness, unit of time and unit of vapour pressure difference between the two sides of the material. To characterize this parameter, the method used is the so-called cup method, presented in NF EN ISO standard 12571. This method consists in imposing a one-dimensional pressure gradient on a sample of thickness e in isothermal conditions (Fig. 5).

$$\delta = \frac{e.\varphi_m}{\Delta P_v}$$

where δ is the water vapour permeability (kg/m.s.pa), φ_m is the mass flow density (g/s.m^2) defined by the mass flow ratio $\emptyset_m$ (g/s) divided by the surface area A (m^2). ΔP_v is the difference of vapour pressure between the two surfaces of the sample (Pa).

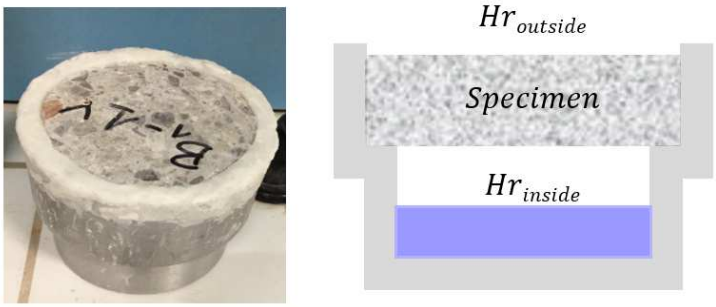

Fig. 5. Principle of the measurement of water vapour permeability by the cup method

In this study, a dry cup test was conducted by imposing a relative humidity of 9% in the cup using a saline solution of potassium hydroxide (KOH). The sample-cup assembly was then placed in a

climatic chamber maintained at 20 °C and 76% relative humidity. Before the test, the 5 cm high cylindrical specimens 11.2 cm in diameter were preconditioned to achieve an overall saturation which corresponds to the average of the relative humidity inside the cup and the relative humidity outside the cup (42.5 %). This average saturation state of the sample is obtained by using the desorption isotherm. Then, mass monitoring is used to determine when the desired saturation state is reached. Finally, a moisture re-distribution is carried out during the same drying time. Monitoring the mass variation by weighing the specimen cup assembly enabled the kinetics to be plotted.

4.3 Simulations and discussion

4.3.1 Analysis of moisture transfer parameters

The moisture transfer parameters were analysed on two materials, BH for series 1 and B1 for series 2. The different evolutions are plotted in Fig. 6 by using the expressions of the different numerical approaches mentioned above to assess the relative permeability to liquid and gas, and R_d, and are compared with the experimental results. This analysis has already been carried out by Ranaivomanana [26] but it is nevertheless important to recall the differences in the evolution of the transfer parameters that have a direct influence on the drying kinetics. So, the relative permeability to liquid evaluated by the model is compared with those calculated by Van Genuchten's model as well as the one modified by Monlouis Bonnaire et al. [15]. For both materials tested, it appears that the porous network model predicts a more significant drop of k_{rl} at high saturation levels than the other models. The contribution of each transport mode is investigated in [7], [58], where it is shown that there is an RH transition region (low to high RH values) from water vapour diffusion dominant to liquid transport dominant, depending on the microstructure of the material, its initial moisture content and the RH boundary condition. This transition region is located in a higher RH range for more porous material and in a lower RH range for less porous material. At high saturation levels, the drying process is essentially governed by the convective contribution of the liquid phase (equation 4). Therefore, it is evident that, for the same intrinsic permeability value (K_l for us), the predicted transfer kinetics will be different depending on the method used to evaluate k_{rl} and k_{rg}. Also, in this contribution, the most important parts are the products $K_l.k_{rl}$ *and* $K_l.k_{rg}$. Although the two parameters differ from one other, the same transfer kinetics can be obtained by different approaches in the short term if the products give the same contribution on the total fluxes. However, a bad set of values inevitably leads to divergences at a given moment.

Then, as the liquid phase becomes discontinuous at lower saturation states, the drying process begins to be governed by the diffusive contribution of the vapour phase (equation 7). The porous network model provides values of the water vapour diffusion reduction factor R_d, which are higher than those calculated with Millington's model, modified by Thiery et al. [8]. Vapour permeability tests were carried out on B1 concrete in accordance with standard NF EN ISO 12571[59]. This was done in order to find the experimental values of R_d by application of standard EN ISO 12572 [60]. The porous

network model showed good agreement with the experimental results while Millington's model, modified by Thiery et al. [8], underestimated resistance effects. The overestimation of R_d from Millington's model could be explained by the fact that this relationship was initially calibrated for granular media, for which the pore size is significantly larger than that of the pores of a concrete where the Knudsen effect is not negligible [8]. An experimental estimate of k_{rg} was obtained from measurements of the intrinsic gas permeability of concrete specimens at different saturation levels using the Klinkenberg approach. These measurements required a pre-treatment phase in which the samples were dried according to the AFPC-AFREM protocol [46] and Carcasses et al. [61]. The porous network model showed good agreement with the experimental results despite a slight overestimation at low saturation levels. Ranaivomanana [50] explains this slight overestimation by the fact that the non-homogeneity of the water content profiles could prevent gas flow through the material by leaving potentially more liquid areas at its core if the re-homogenization of the profile was not complete during pre-conditioning. This would lead to an underestimated experimental measurement of the relative permeability of the gas. This underestimation is less marked on the most permeable materials, allowing easier re-homogenization. Van Genuchten's model modified by Monlouis Bonnaire et al. [15] is found to be close to the experimental points, while Van Genuchten's initial model, validated for soils, gives values that are largely overestimated. It can be observed that, at high saturation levels, neither the initial nor the modified Van Genuchten model considers the fact that the experimental k_{rg} is higher for BH concrete than for BO. This is due to the associated desorption isotherm. To reach the same saturation level, for example 60%, BH needs a lower RH than BO and so greater capillary tension develops in BH, which could lead to more severe damage. Although Mainguy et al. [6] have shown the negligibility of the Darcean gas transfer for cement-based materials (equation 6), as well as the predominance of the transfer in liquid form, it is important to correctly evaluate the transfer parameters from an overall standpoint in order to correctly predict the drying kinetics in the long term.

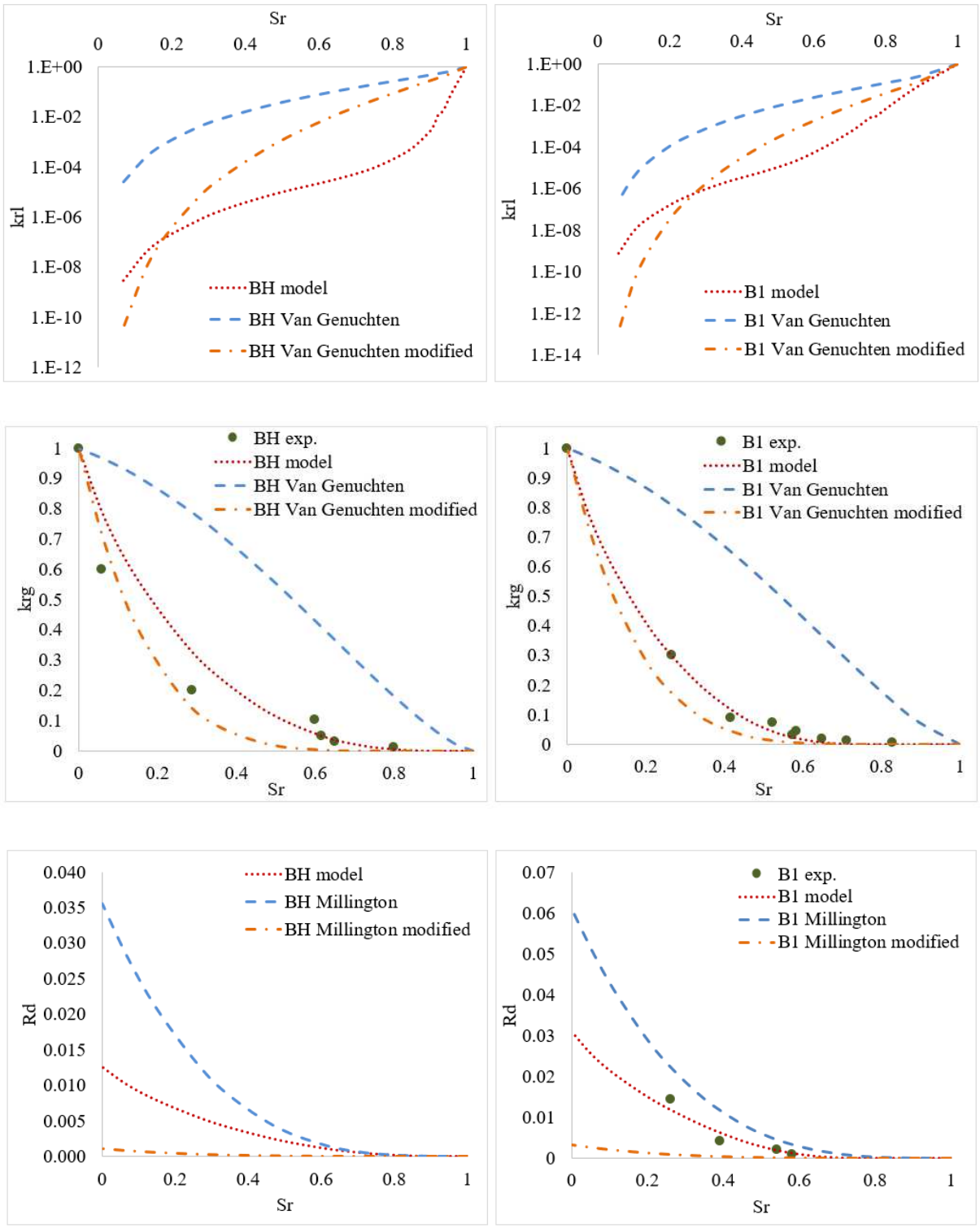

Fig. 6. Comparison between experimental and different theoretical estimating for krl, krg and Rd for BH and B1

4.3.2 Analysis of drying kinetics

At this stage, all the parameters necessary for modelling are known except for the intrinsic permeability of the materials tested. So, as Mainguy et al. [6] did previously, this parameter is calibrated with the value allowing the best restitution of the experimental drying kinetics as a whole (best respecting the kinetics in the short and long term). Many authors [6], [8] have proposed making a

distinction between intrinsic permeabilities to liquid water and gas, since the concept of intrinsic permeability, independently of the nature of the fluid, is not relevant for cementitious materials. The experimental values of intrinsic permeability determined from liquid permeability tests (K_l) and those identified for the materials tested according to the approaches considered are given in Table 4.

In this study:

- mod.1 corresponds to the simulations obtained using the original approach of Van Genuchten and Millington for the evaluation of transfer parameters;

- mod.2 corresponds to the simulations using the modified approach of Van Genuchten and Millington;

- mod.3 corresponds to the simulations obtained using the porous network model to evaluate the transfer parameters.

Table 4: Experimental intrinsic permeabilities and values evaluated by calibration for series 1 and 2 materials

Series reference	1				2			
Material reference	BO	BH	CO	CH	B1	B2	T1	T3
Experimental K_l (x 10^{-20}m²)					9.5	13.7	2.3	1.6
K_l values (mod.1) (x 10^{-20}m²)	0.3	0.05	0.1	0.003	0.3	0.04	0.007	0.0035
K_l values (mod.2) (x 10^{-20}m²)	5	1.5	0.8	0.01	3	0.012	0.02	0.008
K_l values (mod.3) (x 10^{-20}m²)	100	30	130	23	8	0.85	0.37	0.5

The experimental curves of relative mass loss and the equilibrium to be achieved by the materials tested are shown in Fig. 7 and Fig. 8. These figures represent the relative mass losses restored from the three approaches used to evaluate the transfer parameters identified in the previous section. In Fig. 7 (a) and Fig. 7 (b), despite a slight overestimation on the final experimental point (obtained after about 1 year of drying) of mod. 1 and, to a lesser extent, mod. 2, all three approaches correctly predict the kinetics of relative mass loss. Although the deviation at the final experimental point remains acceptable for mod.1 and mod.2, it can be expected that, in the longer term, the kinetics will be shifted farther from the experimental results. This may explain why the equilibrium for BO and CO (Fig. 7 (c) and Fig. 7 (d)) is almost reached at around 700 days for mod.1 while the other curves are still far from equilibrium. It can be noted that the intrinsic permeabilities considered for the simulations have scattered values with several ranges of magnitude. It can also be observed that, on BO and CO, mod.2 and mod.3 are very close, while they differ slightly on BH and CH. Thus, depending on the materials considered, it would seem that mod.2 does not take adequate account of the variations in relative permeability to liquid, thus biasing the simulations on some materials. The lack of data on the experimental intrinsic permeability of this first series of materials leads us to discuss the relevance of the permeability values considered on the materials of series 2 (Table 4). It has already been identified that the fundamental difference between the three approaches to evaluate the transfer parameters is the liquid contribution. k_{rl} is a parameter that cannot be measured experimentally, unlike the intrinsic

permeability to liquid K_l for materials of series 2. Therefore, we can only really validate its relevance by comparing the restored kinetics to that actually observed.

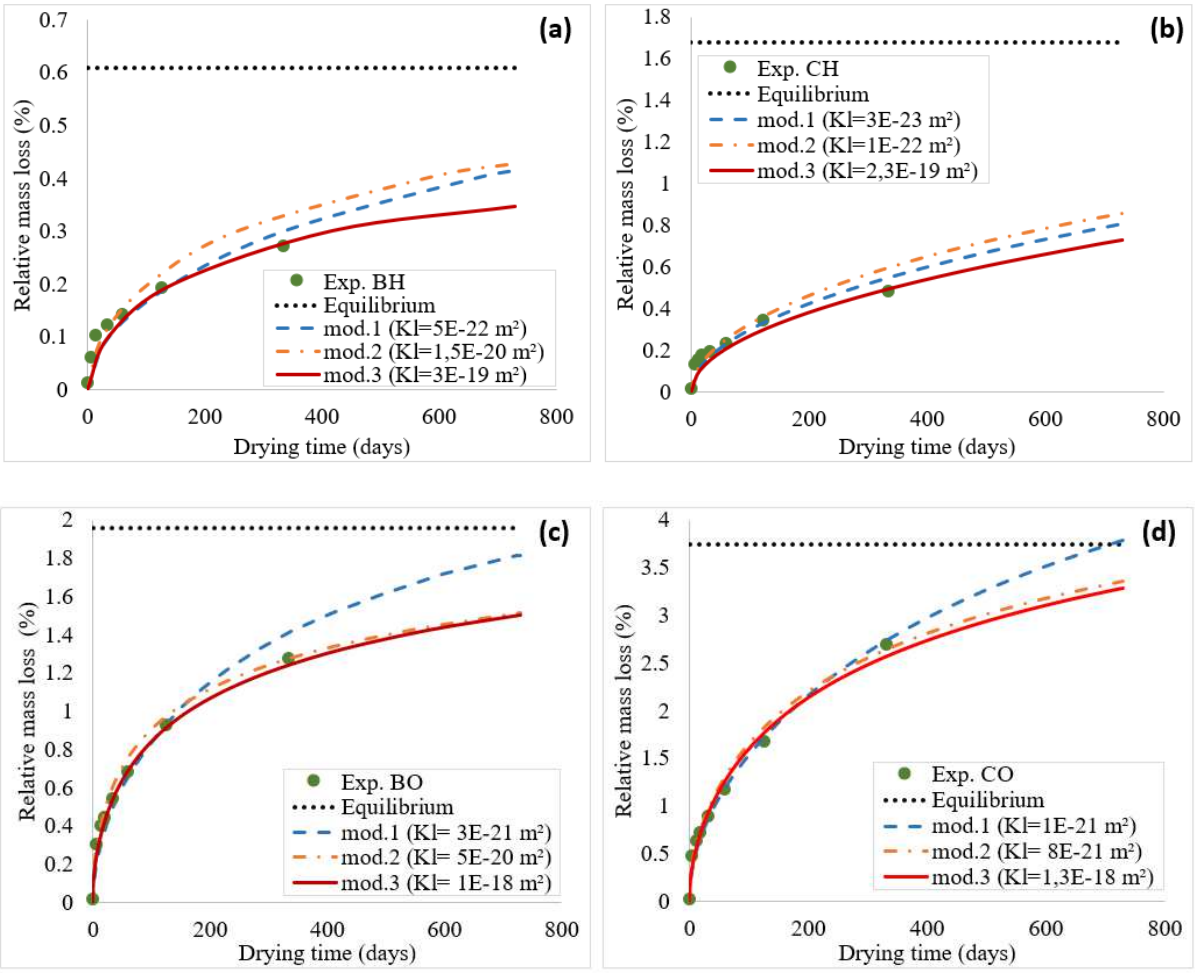

Fig. 7. Confrontations between theoretical approaches and experimental mass losses for the first series of materials

The relative mass losses for the materials of series 2 for a drying time of about 3 years are represented in Fig.6. These experimental kinetics over a longer time period make it possible to identify the limits of mod.1 when it comes to the prediction of long-term drying kinetics. In fact, on B2, T1 and T3, the kinetics are correct up to approximately 200 days and then become too fast compared to the real kinetics. This can be explained by the fact that, besides the overestimation of the liquid contribution despite a very low intrinsic permeability, the diffusion coefficient is also overestimated as mentioned by Thiery et al. [8]. The modified expression of k_{rl} and R_d make it possible to find better long-term kinetics. The analysis of the permeabilities considered for the simulations in relation to the experimental intrinsic permeabilities shows a significant underestimation (a difference of about 2 orders of magnitude) of this parameter for mod.1 and mod.2 (Table 4). Through a comparative study, Zhang et al. [58] concluded that Mainguy's model overestimated the contribution of liquid water due to the use of a slightly higher liquid permeability. Thus, based on the considerable reduction in

intrinsic permeability, it can be concluded that the model based on Van Genuchten's original and modified approaches to the assessment of relative permeabilities reflects a drying process that occurs too quickly in comparison with experimental relative mass losses. The approach using the porous network model (mod.3) is the one that most accurately predicts mass loss kinetics in the long term, with permeabilities closest to those of experiments.

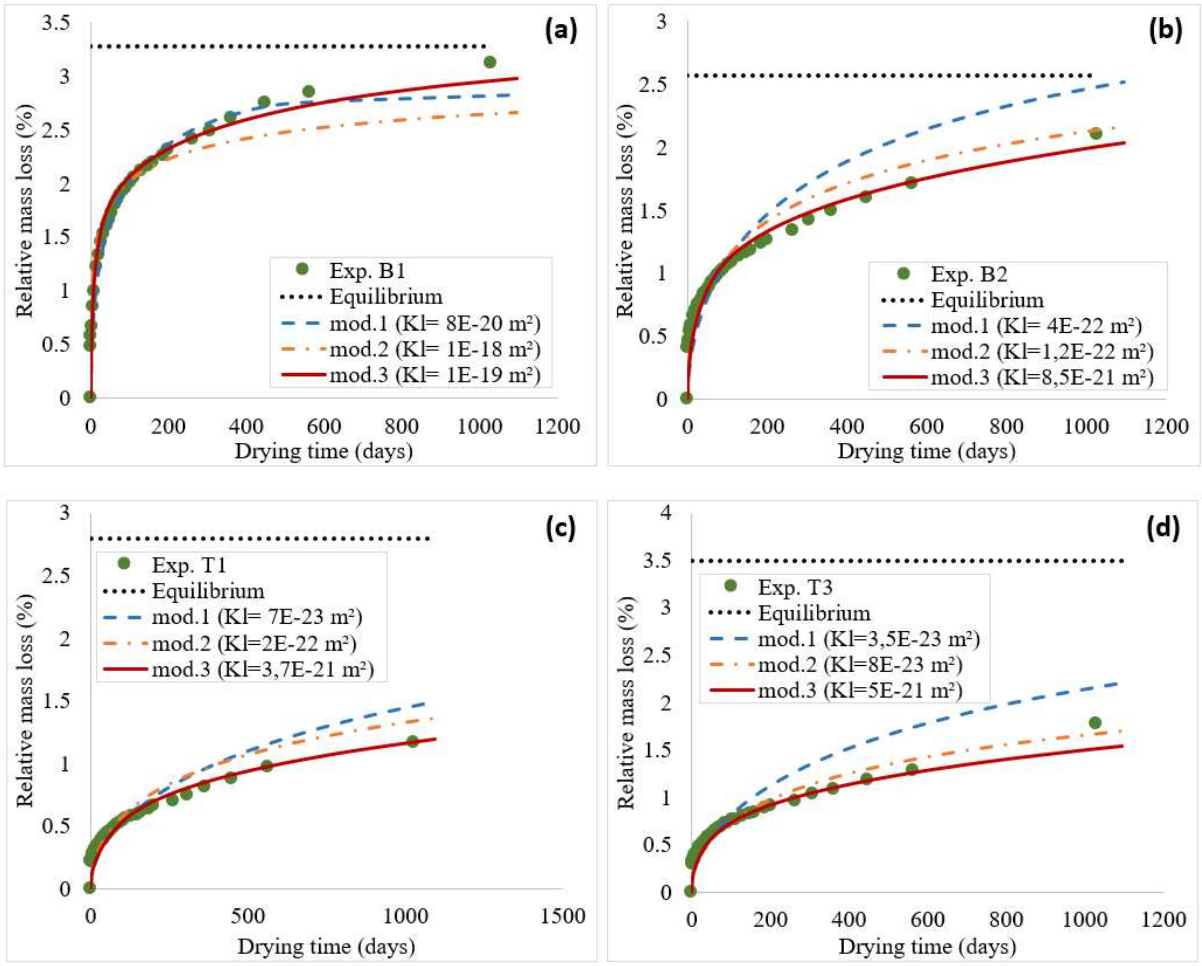

Fig. 8. Confrontations between theoretical approaches and experimental mass losses for the second series of materials

4.3.3 Validation of transfer parameters

In order to validate the transfer parameters, several water transfer tests performed in this study (drying, imbibition, water vapour permeability) were simulated on our materials of series 3 (B1* and B2*). A correctly selected transfer parameter should allow drying, imbibition and water vapour permeability to be correctly simulated. Fig. 9 represents the relative mass losses for the materials of series 3 for a drying time of about five months. Despite a slight overestimation of the initial kinetics, mod. 1 and mod. 3 correctly restore the final relative mass losses up to 153 days. On the other hand, for mod. 2, in addition to the overestimation observed at the beginning of drying, the relative mass losses are underestimated in the longer term for B1*. Here it should be noted that there was a problem with the climatic chamber on these tests during the first 50 days (humidity was higher than the set point). In fact, we noticed a jump in kinetics beyond 50 days on both concretes whose experimental tendencies

are similar. For all the other series without external problem, the experimental kinetics are more correctly simulated.

As observed in previous simulations, the intrinsic permeabilities considered for the different simulation approaches have values scattered over several ranges of magnitude. The experimental values of intrinsic permeability determined from liquid permeability tests (K_l) and those identified for the materials tested according to the approaches considered are given in Table 5. It can be observed that mod.3 considers values close to those observed experimentally while the other two modes tend to underestimate in the case of drying and overestimate in the case of imbibition, for example.

Table 5: Experimental intrinsic permeabilities and values evaluated by calibration for series 3 materials

Series reference	3					
Test	Drying		Imbibition		Water vapour permeability	
Material reference	B1*	B2*	B1*	B2*	B1*	B2*
Experimental K_l (x 10^{-20}m²)	8.2	12	8.2	12	8.2	12
K_l values (mod.1) (x 10^{-20}m²)	0.25	1.3	25	17	0.01	30
K_l values (mod.2) (x 10^{-20}m²)	0.95	0.9	50	30	1000	1200
K_l values (mod.3) (x 10^{-20}m²)	14	15	50	40	9	80

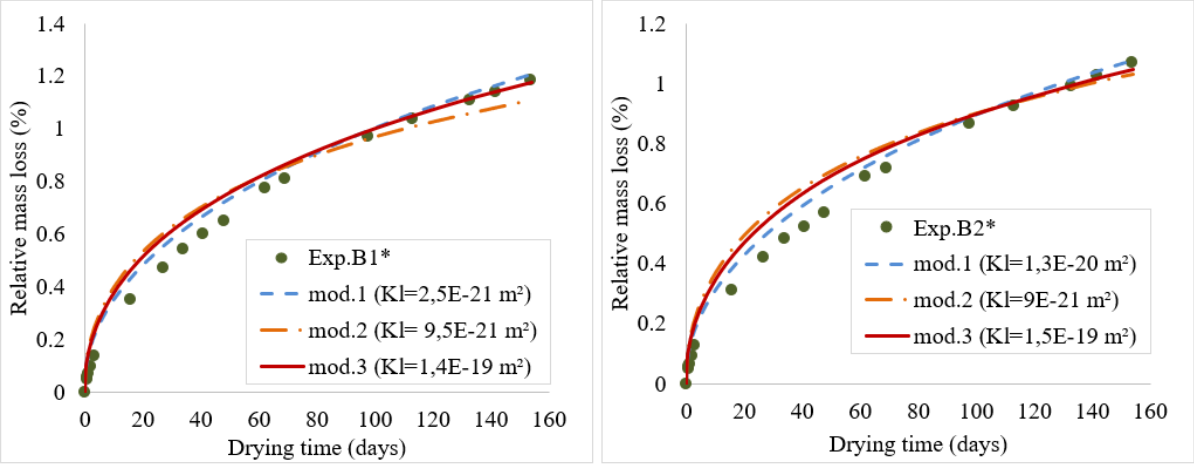

Fig. 9. Confrontations between theoretical approaches and experimental mass losses for the third series of materials

During drying, at each weighing time, local monitoring of resistivity was carried out over the entire height of the specimens. Then, the local saturation degrees were evaluated from the empirical laws of resistivity-degree of saturation established for our materials. Fig. 10 shows the evolution of saturation profiles as a function of the height of the specimens obtained experimentally and from the different modelling approaches. It appears that, for the three approaches, there is good agreement between the experimental resistivity results plotted in terms of saturation profile and the model results. For B1* concrete, mod. 2 and mod. 3 give better restitution of evolutions while mod. 1 presents profiles that are more curved than those observed experimentally. This is particularly evident in the long term at 154 days. However, for B2* concrete, it is less obvious. For mod.3, we observe a discontinuity due to the fall of the isotherm at high saturations. This discontinuity dissipates much faster for B2*, which

has a lower isothermal drop than B1*. Finally, in order to refine the conclusions on these aspects, it would be necessary to confirm the more or less marked linearity of the experimental profiles over greater thicknesses and longer drying times.

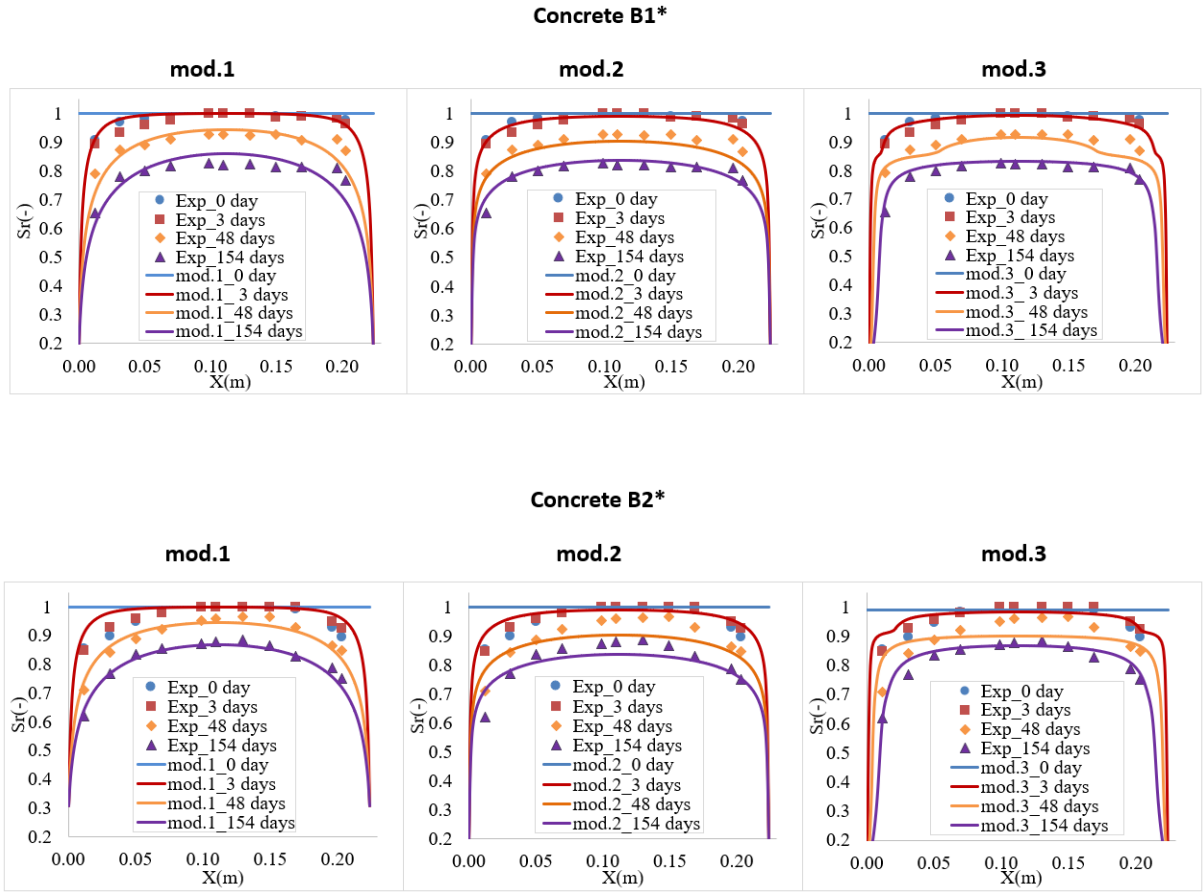

Fig. 10. Confrontations between theoretical approaches and saturation profiles evaluated from resistivity tests for the third series of materials (B1* and B2*)

The results presented in Fig. 11 compare the mass variation of the absorbed water per unit cross section obtained experimentally during capillary imbibition test with the three modelling approaches. These variations are plotted as a function of the square root of imbibition times for B1* and B2*. It appears that, for the three approaches, there is good agreement between the experimental results and the modelling despite a shift in mod. 1 and mod. 2 when B2* reaches the equilibrium level. Compared to drying simulations on these same materials, only mod. 3 is able to restore the right kinetics by keeping intrinsic permeabilities of the same order of magnitude as those considered for drying (Table 5). A slight overestimation of this parameter is nevertheless observed and can be explained by the damage created during drying before the test. It is possible that the pre-conditioning process used to reach the dry state develops damage and cracks that increase permeability. In order to confirm this hypothesis of increasing water permeability on damaged materials, water permeability tests were carried out on B1* before and after drying. The results showed an increase in liquid permeability of 1.3% after drying the sample at 105°C. The input parameters considered in this approach (mod.3)

would therefore be more interesting because they simulate various transfer phenomena correctly from the same data set. However, mod.2 and mod.3 require intrinsic permeabilities close to mod.3 to simulate the test in this case. This results in a difference of up to two orders of magnitude regarding the values considered for the drying simulation.

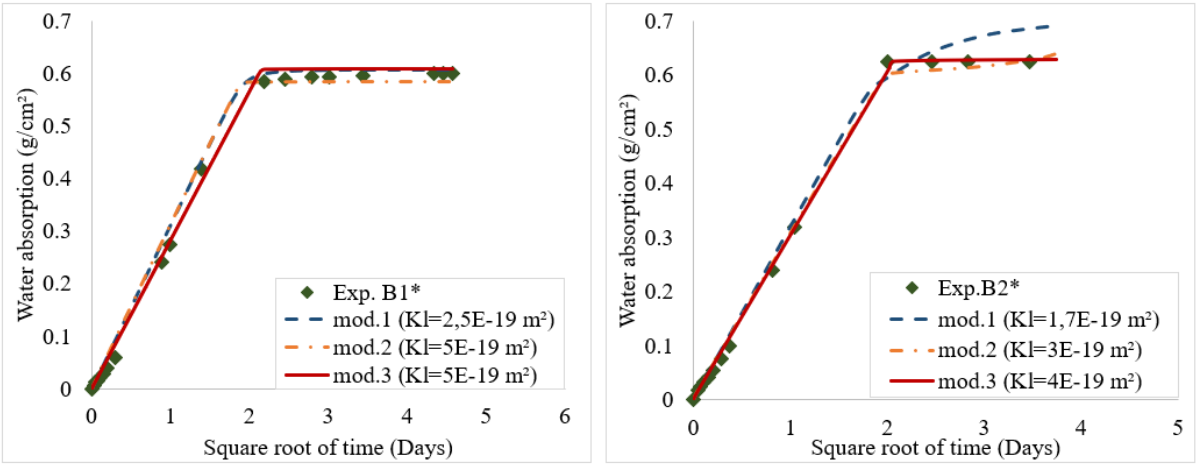

Fig. 11. Confrontations between theoretical approaches and experimental mass loss for the third series of materials

To validate the transfer parameters in the case of a predominantly vapour diffusion transfer, the water vapour permeability test using the cup method was modelled. The boundary conditions imposed on flat surfaces were a relative humidity of 76% on the outside and 9% on the inside of the cup (Fig. 12).

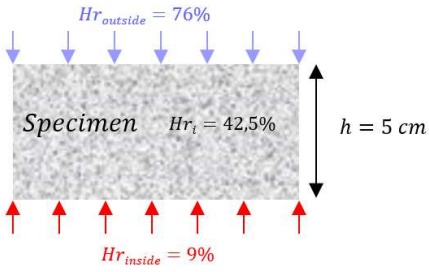

Fig. 12. Boundary conditions imposed in the model

In the case of a water vapour permeability test at intermediate to very low relative humidity (76-9%), the main phenomenon considered is vapour diffusion. Therefore, this test has the interest of highlighting the relevance of the approaches considered for the evaluation of water vapour diffusion reduction factor R_d: the kinetics will be essentially governed by the diffusive contribution of the vapour phase (equation 7). It can be seen in Fig. 13 that mod. 1 has the lowest intrinsic permeabilities for both materials. For B1*, despite a significant underestimation of this permeability compared to the experimental one, the kinetics remain faster because of the water vapour diffusion reduction factor, which presents high values (as simulated on B1, which is similar to B1* (Fig. 6)). On the other hand, mod. 2 significantly overestimates the intrinsic permeability, because the R_d has very low values,

while mod. 3 correctly reproduces the kinetics by keeping the intrinsic permeability values close to the experimental values. Due to the fineness of the porous network of concrete B2, which may not yet be fully described by the porous network model, the R_d value seems underestimated and this leads to a slight overestimation of the intrinsic permeability. In the graphs in Fig. 13, the straight line is only obtained when the steady state is reached. It is coming later on the CEM V due to the fineness and connectivity of its microstructure (less diffusive than the CEM I). It seems that the mod. 1 and mod. 3 correctly simulate this steady state whereas the mod. 2 cannot because of its very low vapour contribution (Fig. 6) which

increases the time to reach the steady state.

As a whole, in addition to the intrinsic permeability, these results allow us to validate the evaluation of the R_d provided by the porous network model while other approaches tend to either overestimate or underestimate this parameter.

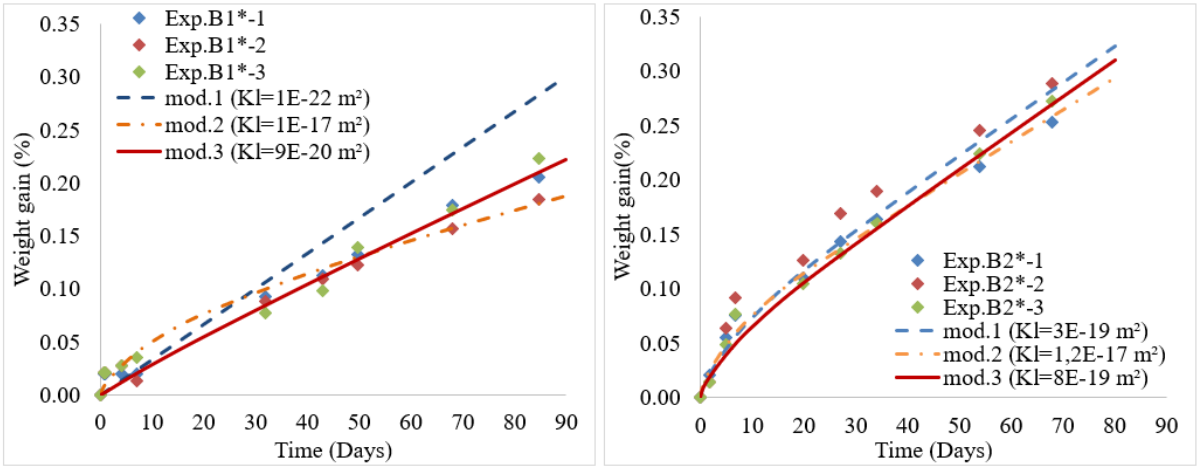

Fig. 13. Confrontations between theoretical approaches and experimental mass losses for the third series of materials

5 Conclusions

The current study has investigated the prediction of moisture transfer for cement-based materials with a model involving dry-air and water vapour components in the gas phase and a liquid-water phase. The prediction of these transfer phenomena depends on the evaluation of the transfer parameters, which can be performed by various methods. More generally, to evaluate the relative permeability to liquid and the water vapour diffusion reduction factor, Van Genuchten's and Millington's models are used respectively. These approaches have been modified by Monlouis Bonnaire et al. [15] and Thiery et al. [8] to adapt them to cement-based materials. A new approach developed by Ranaivomanana et al.[26], [27], based on the porous network and cementitious materials, is proposed in this study to evaluate the parameters required for transfer modelling. This approach is validated based on results obtained from the literature and also on a series of tests involving the main phases of moisture transfer. On both materials tested, the porous network model predicts a more significant drop of k_{rl} at high saturation levels than the other models. The relative permeability to gas evaluated by the porous

network model shows good agreement with the experimental results despite a slight overestimation at low saturation levels. The kinetics of relative mass losses show differences in evolution according to the approach used to evaluate the transfer parameters. The approach proposed for the modelling of moisture transfers in cement-based materials developed by Ranaivomanana et al. and based on a porous network model for the prediction of transfer parameters [26], [27] shows good agreement with experimental evolutions. Similarly, the intrinsic permeabilities considered for this approach are close to the experimental values, whereas the other approaches tend to underestimate (by about two orders of magnitude) this parameter, with significant variations depending on the simulated transfer experiments. Therefore, the comparisons have shown that modelling considering the original and modified Van Genuchten and Millington models uses input data that is unrealistic compared to experimental data available in the literature. However, the kinetics of relative mass loss predicted by these approaches remains correct in the short term, before a relatively large long-term lag. The porous network model taking the hysteresis between sorption and desorption into account and its use in a moisture transfer model is interesting because it can simulate drying and imbibition cycles.

Depending on the approaches used for modelling, the main moisture transport modes are modified, thus explaining the differences observed on all the phenomena modelled. It is therefore necessary to estimate these parameters from models validated on cement-based materials in order to predict moisture transport for this type of materials more correctly.

References

[1] T. Ishida, R. P. Chaube, T. Kishi, et K. Maekawa, « Modeling of pore water content in concrete under generic drying wetting conditions », *Doboku Gakkai Ronbunshu*, vol. 1997, n° 564, p. 199–209, 1997.

[2] Z. P. Bažant et L. J. Najjar, « Nonlinear water diffusion in nonsaturated concrete », *Matér. Constr.*, vol. 5, n° 1, p. 3–20, 1972.

[3] Y. Xi, Z. P. Bažant, et H. M. Jennings, « Moisture diffusion in cementitious materials adsorption isotherms », *Adv. Cem. Based Mater.*, vol. 1, n° 6, p. 248–257, 1994.

[4] R. P. West et N. Holmes, « Predicting moisture movement during the drying of concrete floors using finite elements », *Constr. Build. Mater.*, vol. 19, n° 9, p. 674–681, 2005.

[5] V. Leivo et J. Rantala, « Moisture behaviour of a massive concrete slab with a low temperature floor heating system during the initial drying period », *Constr. Build. Mater.*, vol. 19, n° 4, p. 297–305, 2005.

[6] M. Mainguy, O. Coussy, et V. Baroghel-Bouny, « Role of air pressure in drying of weakly permeable materials », *J. Eng. Mech.*, vol. 127, n° 6, p. 582–592, 2001.

[7] M. Mainguy, O. Coussy, et R. Eymard, « Modelisation des transferts hydriques isothermes en milieu poreux. Application au sechage des materiaux a base de ciment », *ETUDES Rech. Lab.*

PONTS CHAUSSEES - Ser. OUVRAGES ART, n° OA 32, juill. 1999, Consulté le: janv. 25, 2019. [En ligne]. Disponible sur: https://trid.trb.org/view/958954.
[8] M. Thiery, V. Baroghel-Bouny, N. Bourneton, G. Villain, et C. Stéfani, « Modélisation du séchage des bétons: analyse des différents modes de transfert hydrique », *Rev. Eur. Génie Civ.*, vol. 11, n° 5, p. 541–577, 2007.
[9] Y. Mualem, « A new model for predicting the hydraulic conductivity of unsaturated porous media », *Water Resour. Res.*, vol. 12, n° 3, p. 513–522, 1976.
[10] M. T. Van Genuchten, « A closed-form equation for predicting the hydraulic conductivity of unsaturated soils 1 », *Soil Sci. Soc. Am. J.*, vol. 44, n° 5, p. 892–898, 1980.
[11] D. Breysse et B. Gerard, « Modelling of permeability in cement-based materials: Part 1-Uncracked medium », *Cem. Concr. Res.*, vol. 27, n° 5, p. 761–775, 1997.
[12] A. Aït-Mokhtar, O. Amiri, P. Dumargue, et S. Sammartino, « A new model to calculate water permeability of cement-based materials from MIP results », *Adv. Cem. Res.*, vol. 14, n° 2, p. 43–49, 2002.
[13] F. A. Dullien, « New network permeability model of porous media », *AIChE J.*, vol. 21, n° 2, p. 299–307, 1975.
[14] G. Ye, P. Lura, et van K. van Breugel, « Modelling of water permeability in cementitious materials », *Mater. Struct.*, vol. 39, n° 9, p. 877–885, 2006.
[15] J. P. Monlouis-Bonnaire, J. Verdier, et B. Perrin, « Prediction of the relative permeability to gas flow of cement-based materials », *Cem. Concr. Res.*, vol. 34, n° 5, p. 737–744, 2004.
[16] O. Amiri, A. Aït-Mokhtar, et M. Sarhani, « Tri-dimensional modelling of cementitious materials permeability from polymodal pore size distribution obtained by mercury intrusion porosimetry tests », *Adv. Cem. Res.*, vol. 17, n° 1, p. 39–45, 2005.
[17] G. S. Park et J. Crank, « Diffusion in polymers », 1968.
[18] A. Z. Akcasu, « Temperature and concentration dependence of diffusion coefficient in dilute solutions », *Polymer*, vol. 22, n° 9, p. 1169–1180, 1981.
[19] R. J. Millington, « Gas diffusion in porous media », *Science*, vol. 130, n° 3367, p. 100–102, 1959.
[20] A. V. Saetta, R. V. Scotta, et R. V. Vitaliani, « Analysis of chloride diffusion into partially saturated concrete », *Mater. J.*, vol. 90, n° 5, p. 441–451, 1993.
[21] P. C. Philippi et H. A. de Souza, « Modelling moisture distribution and isothermal transfer in a heterogeneous porous material », *Int. J. Multiph. Flow*, vol. 21, n° 4, p. 667–691, 1995.
[22] T. Ishida, K. Maekawa, et T. Kishi, « Enhanced modeling of moisture equilibrium and transport in cementitious materials under arbitrary temperature and relative humidity history », *Cem. Concr. Res.*, vol. 37, n° 4, p. 565–578, 2007.
[23] Z. Jiang, Y. Xi, X. Gu, Q. Huang, et W. Zhang, « Modelling of water vapour sorption hysteresis of cement-based materials based on pore size distribution », *Cem. Concr. Res.*, vol. 115, p. 8-19, janv. 2019, doi: 10.1016/j.cemconres.2018.09.015.
[24] J. M. de Burgh, S. J. Foster, et H. R. Valipour, « Prediction of water vapour sorption isotherms and microstructure of hardened Portland cement pastes », *Cem. Concr. Res.*, vol. 81, p. 134–150, 2016.
[25] T. C. Hansen, « Physical structure of hardened cement paste. A classical approach », *Mater. Struct.*, vol. 19, n° 6, p. 423–436, 1986.
[26] H. Ranaivomanana, J. Verdier, A. Sellier, et X. Bourbon, « Toward a better comprehension and modeling of hysteresis cycles in the water sorption–desorption process for cement based materials », *Cem. Concr. Res.*, vol. 41, n° 8, p. 817–827, 2011.
[27] H. Ranaivomanana, J. Verdier, A. Sellier, et X. Bourbon, « Prediction of relative permeabilities and water vapor diffusion reduction factor for cement-based materials », *Cem. Concr. Res.*, vol. 48, p. 53–63, 2013.
[28] C. Hall, « Water sorptivity of mortars and concretes: a review », *Mag. Concr. Res.*, vol. 41, n° 147, p. 51-61, juin 1989, doi: 10.1680/macr.1989.41.147.51.
[29] C. Hammecker et D. Jeannette, « Modelling the capillary imbibition kinetics in sedimentary rocks: Role of petrographical features », *Transp. Porous Media*, vol. 17, n° 3, p. 285–303, 1994.

[30] W. J. McCarter, H. Ezirim, et M. Emerson, « Properties of concrete in the cover zone: water penetration, sorptivity and ionic ingress », *Mag. Concr. Res.*, vol. 48, n° 176, p. 149-156, sept. 1996, doi: 10.1680/macr.1996.48.176.149.
[31] M. Saleem, M. Shameem, S. E. Hussain, et M. Maslehuddin, « Effect of moisture, chloride and sulphate contamination on the electrical resistivity of Portland cement concrete », *Constr. Build. Mater.*, vol. 10, n° 3, p. 209-214, avr. 1996, doi: 10.1016/0950-0618(95)00078-X.
[32] J.-K. Su, C.-C. Yang, W.-B. Wu, et R. Huang, « Effect of moisture content on concrete resistivity measurement », *J. Chin. Inst. Eng.*, vol. 25, n° 1, p. 117-122, janv. 2002, doi: 10.1080/02533839.2002.9670686.
[33] R. Du Plooy, S. P. Lopes, G. Villain, et X. Derobert, « Development of a multi-ring resistivity cell and multi-electrode resistivity probe for investigation of cover concrete condition », *NDT E Int.*, vol. 54, p. 27–36, 2013.
[34] S. Bonnet, « Influence du chlore sur le comportement à l'équilibre et sur les propriétés de transfert de matériaux du génie civil », PhD Thesis, Toulouse, INSA, 1997.
[35] O. Francy, « Modélisation de la pénétration des ions chlorures dans les mortiers partiellement saturés en eau », PhD Thesis, Toulouse 3, 1998.
[36] V. Baroghel-Bouny, M. Mainguy, T. Lassabatere, et O. Coussy, « Characterization and identification of equilibrium and transfer moisture properties for ordinary and high-performance cementitious materials », *Cem. Concr. Res.*, vol. 29, n° 8, p. 1225-1238, août 1999, doi: 10.1016/S0008-8846(99)00102-7.
[37] B. Perrin, V. B. Bouny, et L. Chemloul, « Méthodes de détermination de la diffusivité hydrique de pâtes de ciments durcies », *Mater. Struct.*, vol. 31, n° 4, p. 235–241, 1998.
[38] J.-F. Daian, « Processus de condensation et de transfert d'eau dans un matériau meso et macroporeux: étude expérimentale du mortier de ciment. », PhD Thesis, Université Scientifique et Médicale de Grenoble, 1986.
[39] D. Xin, D. G. Zollinger, et G. D. Allen, « An approach to determine diffusivity in hardening concrete based on measured humidity profiles », *Adv. Cem. Based Mater.*, vol. 2, n° 4, p. 138–144, 1995.
[40] O. Coussy, R. Eymard, et T. Lassabatere, « Constitutive modeling of unsaturated drying deformable materials », *J. Eng. Mech.*, vol. 124, n° 6, p. 658–667, 1998.
[41] O. Coussy, *Mechanics of porous continua*. Wiley, 1995.
[42] D. A. De Vries et A. J. Kruger, « On the value of the diffusion coefficient of water vapour in air », in *Proc. Of Colloque Int. Du CNRS*, 1966, p. 61u72.
[43] B. Pradhan, M. Nagesh, et B. Bhattacharjee, « Prediction of the hydraulic diffusivity from pore size distribution of concrete », *Cem. Concr. Res.*, vol. 35, n° 9, p. 1724–1733, 2005.
[44] S. Bejaoui et B. Bary, « Modeling of the link between microstructure and effective diffusivity of cement pastes using a simplified composite model », *Cem. Concr. Res.*, vol. 37, n° 3, p. 469–480, 2007.
[45] F. Adenot, « Durabilité du béton: caractérisation et modélisation des processus physiques et chimiques de dégradation du ciment », PhD Thesis, Orléans, 1992.
[46] AFPC, « Méthodes recommandées pour la mesure des grandeurs associées à la durabilité », *C. r. Journ. Tech. AFPC-AFREM Durabilité Bétons*, 1997.
[47] S. Brunauer, P. H. Emmett, et E. Teller, « Adsorption of gases in multimolecular layers », *J. Am. Chem. Soc.*, vol. 60, n° 2, p. 309–319, 1938.
[48] Q. Wu, T. Rougelot, N. Burlion, et X. Bourbon, « Experimental study of the water desorption and drying shrinkage of cement-based materials with thin slices », in *CONCREEP 10*, 2015, p. 1099–1108.
[49] V. Baroghel-Bouny, « Caractérisation microstructurale et hydrique des pâtes de ciment et des bétons ordinaires et à très hautes performances », PhD Thesis, Ecole Nationale des Ponts et Chaussées, 1994.

[50] H. Ranaivomanana, « Tranferts dans les milieux poreux réactifs non saturés: application à la cicatrisation de fissure dans les matériaux cimentaires par carbonatation », PhD Thesis, Université de Toulouse, Université Toulouse III-Paul Sabatier, 2010.
[51] V. Baroghel-Bouny, « Water vapour sorption experiments on hardened cementitious materials: Part I: Essential tool for analysis of hygral behaviour and its relation to pore structure », *Cem. Concr. Res.*, vol. 37, n° 3, p. 414–437, 2007.
[52] V. Baroghel-Bouny, « Water vapour sorption experiments on hardened cementitious materials. Part II: Essential tool for assessment of transport properties and for durability prediction », *Cem. Concr. Res.*, vol. 37, n° 3, p. 438–454, 2007.
[53] G. Villain, V. Baroghel-Bouny, C. Kounkou, et C. Hua, « Mesure de la perméabilité aux gaz en fonction du taux de saturation des bétons », *Rev. Fr. Génie Civ.*, vol. 5, n° 2-3, p. 251–268, 2001.
[54] T. L. P. Hang, « Les bétons bas pH : comportements initial et différé sous contraintes externes », phdthesis, Université Paul Sabatier - Toulouse III, 2015.
[55] K. Gowers et S. Millard, « Measurement of concrete resistivity for assessment of corrosion », *ACI Mater. J.*, vol. 96, n° 5, 1999.
[56] S. Laurens, J. P. Balayssac, J. Rhazi, G. Klysz, et G. Arliguie, « Non-destructive evaluation of concrete moisture by GPR: experimental study and direct modeling », *Mater. Struct.*, vol. 38, n° 9, p. 827–832, 2005.
[57] H. Sogbossi, J. Verdier, et S. Multon, « Permeability and damage of partially saturated concrete exposed to elevated temperature », *Cem. Concr. Compos.*, vol. 109, p. 103563, 2020.
[58] Z. Zhang, M. Thiéry, et V. Baroghel-Bouny, « Analysis of moisture transport in cementitious materials and modelling of drying-wetting cycles », *Proc SSCS Aix-En-Provence Fr.*, 2012.
[59] N. E. ISO 12571, *Hygrothermal Performance of Building Materials and Products, Determination of Hygroscopic Sorption Properties*. 2000.
[60] E. ISO 12572, « 12572: Hygrothermal performance of building materials and products-Determination of water vapour transmission properties (ISO 12572: 2001) », *CEN Eur. Comm. Stand. Bruss. 27p*, 2001.
[61] M. Carcasses, A. Abbas, J.-P. Ollivier, et J. Verdier, « An optimised preconditioning procedure for gas permeability measurement », *Mater. Struct.*, vol. 35, n° 1, p. 22–27, 2002.